Physica 128B (1985) 13–25
North-Holland, Amsterdam

RELAXATION BEHAVIOUR AT THE SPIN–FLOP PHASE TRANSITION IN THE QUASI-1D ANTIFERROMAGNET $CsMnCl_3 \cdot 2H_2O$

M. CHIRWA*, J.L. TOP and J. FLOKSTRA
Department of Applied Physics, Twente University of Technology, P.O. Box 217, 7500 AE Enschede, The Netherlands

Received 14 May 1984

The low-frequency relaxation behaviour of the linear-chain antiferromagnet $CsMnCl_3 \cdot 2H_2O$ at the spin–flop transition has been determined from dynamic susceptibility measurements on a single crystal placed in direct contact with liquid helium. The experiments were performed between 1.4 and 4.2 K in the frequency range 0.1 Hz–3.0 kHz with a frequency-sweeping SQUID susceptometer. Below $T_\lambda = 2.17$ K, the relaxation rate τ^{-1} manifests an exponential temperature dependence, $\tau^{-1} = \omega_0 e^{-E/kT}$, where $E/k = 3.19 \pm 0.04$ K is approximately equal to the magnitude of the intrachain exchange interaction constant J_a/k. Above T_λ the apparent deviation from the exponential behaviour has been explained satisfactorily by using the thermal conduction model of relaxation. The field-dependent factor ω_0 is directly proportional to the ratio of the adiabatic χ_s to the isothermal χ_T susceptibilities.

1. Introduction

A phase transition between two ordered magnetic phases is usually characterized by the occurrence of an intermediate state in which the two ordered phases co-exist as domains. Such domain structures, whose formation is energetically favourable, exist in a small field range (the intermediate state) when a sufficiently large magnetic field is applied parallel to the easy axis of magnetization. In a weakly anisotropic Heisenberg antiferromagnet this phase transition is the spin–flop transition, at which the co-existing antiferromagnetic (AF) and spin–flop (SF) phases are separated by 90° domain walls [1]. In a strongly anisotropic Ising antiferromagnet, 180° domain walls separate the AF and, for example, the ferrimagnetic (FI) phases at the corresponding metamagnetic transition.

The existence of the intermediate state at the spin–flop transition has been ascertained experimentally for several antiferromagnets including MnF_2, $NiWO_4$, $CuCl_2 \cdot 2H_2O$ and $CsMnCl_3 \cdot 2H_2O$ [2–4]. Studies of optical absorption, Faraday rotation, Barkhausen effects and NMR were used to observe the intermediate state in these compounds. For MnF_2 the corresponding domain structure was observed [2] with photographic techniques involving selective optical-absorption of the AF and SF phases.

A variety of physical properties such as susceptibility, magnetization, magneto-striction, thermal expansion, thermal conductivity and ultrasonic attenuation, which exhibit a more or less sudden change of behaviour at the AF–SF phase transition, are used to study the spin–flop transition [5]. However, there are very few investigations, of susceptibility for example, at the spin–flop transition in the presence of a small oscillating magnetic field. The reason is that the conventional (mutual inductance) field-sweep technique is not really suitable for measuring the dynamic susceptibility $\chi = \chi' - i\chi''$ at phase transitions, especially at the AF–SF transition, where χ is very sensitive to small variations in temperature, magnetic field, sample position and orientation. With the automatic frequency-sweeping SQUID susceptometer [6] recently developed in our laboratory, used in combination with a digital phase sensitive detection and data acquisition system [7], it is now possible to perform, directly and with high sensitivity, an accurate and rapid measurement of the frequency dependence of χ.

Our investigation of the spin–flop transition is

* Permanent address: Physics Department, University of Zambia, P.O. Box 32379, Lusaka, Zambia.

concerned with the dynamic behaviour of the domain walls between the AF and SF phases in the presence of a perturbing small oscillating magnetic field. This domain wall relaxation appears to be a low-frequency (<10 kHz according to Rohrer [8]) relaxation phenomenon exhibiting an exponential temperature T dependence of the relaxation time τ given by [9]

$$\tau^{-1} = \omega_0 \exp(-E/kT), \quad (1)$$

where E is the activation energy for domain wall motion and k is the Boltzmann constant. The coefficient ω_0 depends on the relative fraction of the co-existing ordered phases. According to Tinkham's phase-nucleation theory [10] for metamagnetic transitions in low-dimensional magnetic systems [11], the activation energy $E = |J|$ for surface or impurity-site nucleation or $E = 2|J|$ in the case of volume (inner site) nucleation. Here J is the intrachain exchange interaction constant. In a previous experimental investigation [9] of the spin–flop transition relaxation in $CsMnBr_3 \cdot 2H_2O$, the relaxation time was found to increase exponentially with decreasing temperature according to eq. (1) with $E/k \sim 3.6$ K. This value of E is of the same order of magnitude as the intrachain exchange constant for this compound, indicating a probable phase-nucleation behaviour for the relaxation.

The measurements on $CsMnBr_3 \cdot 2H_2O$ [9] above the lambda transition $T_\lambda (= 2.17\ \text{K})$ of liquid helium yielded relaxation curves which were markedly different from those predicted by the Casimir-du Pré [12] theory. This apparent behaviour, which is an indication of the strong influence of the thermal and geometrical properties of the sample and environment, can be easily accounted for in the thermal conduction model [13] description of relaxation. Successful applications of this model have already been performed [14, 15]. A similar analysis for $CsMnBr_3 \cdot 2H_2O$ has not yet been completed because of insufficient thermal data at the spin–flop transition for this compound. As a result only the time constants for $T < T_\lambda$ in ref. [9], where the environmental influence is weak, were used to verify eq. (1).

This paper presents the results of an extensive experimental study of the spin–flop relaxation behaviour for $CsMnCl_3 \cdot 2H_2O$. The experiments were performed in the frequency range 0.1 Hz–3 kHz between 1.4 and 4.2 K using the automatic frequency-sweeping SQUID susceptometer. By using the thermal conduction model for measurements above T_λ it has been demonstrated that for $CsMnCl_3 \cdot 2H_2O$ eq. (1) is possibly valid for temperatures above T_λ as well. The relevant magnetic properties of $CsMnCl_3 \cdot 2H_2O$ are discussed in section 2. This is followed by a brief outline of the experimental procedures in section 3. In sections 4 and 5 the experimental results and discussion, respectively, are presented.

2. Magnetic properties of $CsMnCl_3 \cdot 2H_2O$

2.1. Magnetic and crystallographic structure

The quasi-one dimensional Heisenberg antiferromagnetic compound $CsMnCl_3 \cdot 2H_2O$ has an orthorhombic crystallographic structure with space group Pcca [16]. The chemical unit cell contains four formula units and has dimensions $a = 9.060$ Å, $b = 7.285$ Å and $c = 11.455$ Å. Four Cl^- ions and two water molecules form a distorted octahedron surrounding the magnetic Mn^{2+} ion. Two of the Cl^- ions are shared by neighbouring Mn^{2+} ions, thus forming a slightly zig-zag Mn^{2+}–Cl^-–Mn^{2+} chain which extends indefinitely in the crystallographic a direction. In the b and c directions the chains are separated from each other by non-magnetic atoms. The Mn^{2+} ion is in the ^6S ground state with a magnetic moment corresponding to spin $S = 5/2$ and isotropic $g = 2.00$. In the AF state the magnetic space group is $P_{2b}c'ca'$ as determined from NMR and neutron diffraction studies [17, 18]. This magnetic space group implies a magnetic unit cell that is twice as long as the chemical one along the b axis and antiferromagnetic exchange interactions along the three crystallographic axes. The b, c and a axes are respectively the easy, the intermediate and hard directions of magnetization in the antiferromagnetically ordered phase.

2.2. One-dimensionality

The one-dimensional character of $CsMnCl_3 \cdot 2H_2O$ above its three-dimensional ordering temperature T_N is evident from the magnetic and crystallographic structure (section 2.1), the broad maxima in the susceptibility and magnetic heat capacity versus temperature curves at $T > T_N$ and the low entropy gain ($\sim 14\%$) for $0 < T \leq T_N$ [19–23]. Further evidence of linear-chain antiferromagnetism is provided by the neutron diffraction experiments [18] which show that the development of substantial spin–spin correlations along the a axis of $CsMnCl_3 \cdot 2H_2O$ begins at temperatures as high as $10T_N$. The intrachain J_a and the interchain J_b and J_c exchange interaction constants for this compound have been determined using different techniques (see table I for references). On the average $J_a/k = -3.20$ K, $J_b/J_a \sim 6 \times 10^{-3}$ and $J_c/J_a \sim 16 \times 10^{-3}$.

2.3. Magnetic phase diagram and anisotropy

The magnetic phase diagrams of $CsMnCl_3 \cdot 2H_2O$ have been studied extensively both theoretically and experimentally [21, 30–33]. For H parallel to the easy (b) axis the H–T phase diagram displays the paramagnetic (PM), the AF and SF phases with $T_N = 4.886 \pm 0.005$ K and bicritical point $T_b = 4.354$ K, $\mu_0 H_b = 2.0144$T [33]. In the AF phase the magnetic moments are aligned parallel to the b axis whereas in the SF phase they lie nearly parallel to the c axis. For $T < 0.9T_b$ the spin–flop field H_{SF} exhibits a linear temperature dependence:

$$\mu_0 H_{SF} = c_1 + c_2 T. \tag{2}$$

Values of the constants c_1 and c_2 are given in table II.

$CsMnCl_3 \cdot 2H_2O$ has a uni-axial anisotropy relative to the a axis at temperatures above 10 K [34]. Below this temperature the anisotropy is orthorhombic with $K_1/K_2 \sim 0.31$ [21, 35], where K_1 and K_2 are the anisotropy energies in the c and a directions respectively. Dipolar interactions are chiefly responsible for the anisotropy.

3. Experimental procedure

Measurements of the dynamic susceptibility χ using the 5 T frequency-sweeping SQUID susceptometer [6, 7] were carried out on a 10.9 mg single crystal of $CsMnCl_3 \cdot 2H_2O$ placed in direct contact with liquid helium. The dimensions of

Table I
The intrachain J_a and interchain J_b, J_c exchange interaction constants for $CsMnCl_3 \cdot 2H_2O$. C_M is the magnetic heat capacity at constant magnetization M; χ is the susceptibility.

J_a/k (K)	J_b/J_a	J_c/J_a	Source
−3.115, −3.00			$\chi(T)$ at $T > T_N$ [19]
−3.39			$\chi_\perp$ [20]
−3.14			$\chi(T)$ at $T > T_N$ [21]
−3.3 ± 0.3			C_M for $12 < T < 52$ K [22]
−3.0 ± 0.2/0.4			$C_M(T)$ with different model for C_L [23]
−3.53 ± 0.04	$(J_b + J_c)/J_a = 6.9 \times 10^{-3}$		neutron scattering [24]
	$2 \times 10^{-2} - 2.6 \times 10^{-4}$	$2.0 \times 10^{-2} - 2.6 \times 10^{-2}$	ESR line shape [25]
	$\ll 3.5 \times 10^{-2}$	3.5×10^{-2}	proton spin relaxation at $T = 300$ K [26]
−3.2	$\sim 1.3 \times 10^{-3}$	6.3×10^{-3}	$\chi(T), M(T)$ spin wave analysis [27]
−3.0	$(J_b + J_c)/J_a = 8 \times 10^{-3}$		$C_M(T)$ spin wave analysis [28]
−3.13 ± 0.15			optical birefringence [29]
−3.17 ± 0.03			$\chi_\parallel$ ($\omega/2\pi = 70$ Hz) [30]

Table II
Parameters c_1 and c_2 for linear temperature dependence of the spin–flop magnetic field H_{SF}: $\mu_0 H_{SF} = c_1 + c_2 T$

c_1(T)	c_2(T K^{-1})	Source
1.64	0.084	magnetization in static field [21]
1.610	0.102	inflection pts. of isentropes [31]
1.6485	0.0866	static parallel susceptibility [30]
1.63	0.0873	$\chi'(H)$, our measurements

the crystal along directions parallel to the *a*, *b* and *c* axes were 3.0, 1.9 and 0.7 mm, respectively. We used the sample-holder rotation mechanism [9] to rotate the sample completely about its *c* axis, with the field direction always lying in the *ab* plane. The crystal was oriented with the magnetic field parallel to the easy (*b*) axis by using the sine wave-like angular dependence of the zero-field dynamic susceptibility χ_0 measured in the AF phase. The parallel ($H \| b$ axis) and perpendicular ($H \| a$ axis) orientations were easily located as they coincide with the minima and maxima in the χ_0 rotation curves, respectively.

The AF–SF phase boundary in the H–T plane was approached in two ways. The first method was to measure the dynamic susceptibility as a function of the magnetic field at discrete values of H at fixed temperature T. Continuous field-sweep measurements are not possible without filtering the substantial noise from the magnet's power amplifier which disturbs the operation of the SQUID. The second method was to measure the dynamic susceptibility continuously as a function of temperature at a constant but sufficiently high magnetic field. The latter method proved to be more suitable in determining the maximum χ in the AF–SF region. The frequency dependence of χ was then measured at constant temperature in constant magnetic field. Except for the results in section 4.1.1, all the measurements presented here were performed for $h_p \leq 10$ A m^{-1} as the amplitude of the oscillating magnetic field component.

4. Experimental results on $CsMnCl_3 \cdot 2H_2O$

In general the dynamic susceptibility χ is a function of the magnetic field vector $\boldsymbol{H}$ relative to the crystal axes, the temperature T, the frequency $\omega/2\pi$ and amplitude h_p of the small oscillating magnetic field component. It also depends on crystal shape (demagnetization) and the nature of the environment (for example liquid or gaseous helium, vacuum, etc.). We discuss the field and temperature dependence of χ in section 4.1 and then analyse the frequency dependence of χ, and therefore the relaxation behaviour, at the spin–flop transition in section 4.2. The influence of the environment is discussed in section 4.3.

4.1. Field and temperature dependence of dynamic susceptibility

4.1.1. $\chi(H)$ near the AF–SF phase transition

Fig. 1 shows an example of the variation of the dispersion χ' and absorption χ'' as functions of the magnetic field H obtained at $T = 2.776$ K for $\omega/2\pi = 127$ Hz and $h_p = 33$ A m^{-1}. The peaks in the $\chi'(H)$ and $\chi''(H)$ curves, centred at $H = H_{SF} = 1.492 \times 10^6$ A m^{-1}, identify the intermediate state between the lower-field AF and the higher-field SF phases. The H_{SF} values obtained in this manner were used to verify the linear temperature dependence of H_{SF} (eq. (2)). The results are in good

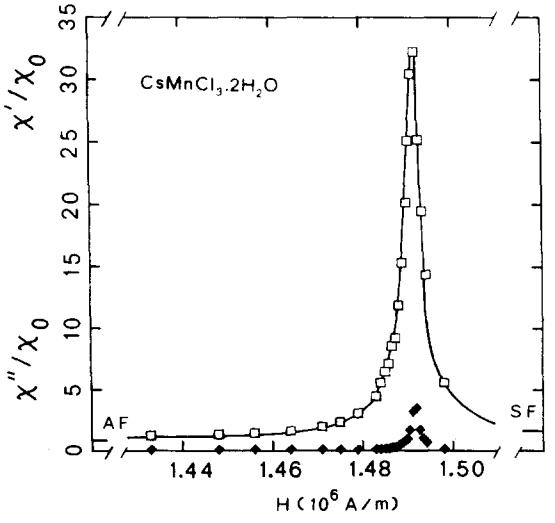

Fig. 1. Magnetic-field dependence of the dispersion χ' (open symbols) and the absorption χ'' (closed symbols), relative to χ' at $H = 0$ (χ_0), showing the AF–SF phase transition in $CsMnCl_3 \cdot 2H_2O$ at $T = 2.776$ K for $\omega/2\pi = 127$ Hz and $h_p = 33$ A m^{-1}.

agreement with previous measurements (see table II). The half width ΔH at half height of the peak in the $\chi'(H)$ curve is about 2.5×10^3 A m^{-1} so that $h_p/\Delta H \sim 10^{-2}$.

In the AF state χ is independent of H and is equal to its zero-field value χ_0. In the SF state χ is constant but a little larger than χ_0. At the spin–flop transition $\chi'(H)/\chi_0 \gg 1$ and has its maximum value when $\chi' = \chi_T$ and minimum value when $\chi' = \chi_s$ (see subsection 4.1.2). Fig. 1 also shows that χ'' at $\omega/2\pi = 127$ Hz is zero in both the AF and SF phases but in the intermediate state between the two ordered phases a small peak has been observed. This clearly demonstrates the occurrence of a low-frequency relaxation at the AF–SF phase transition which is absent in the ordered phases.

4.1.2. $\chi(T)$ in the AF–SF intermediate state

At a sufficiently large field H the dynamic susceptibility χ measured as a function of temperature exhibits a peak associated with the AF–SF intermediate state. In fig. 2 we show the temperature dependence of the dispersion χ' near $T = 2.00$ K at $H = 1.44 \times 10^6$ A m^{-1} for $\omega/2\pi =$ 29.2, 141 and 2085 Hz. The sharpness and height of the $\chi'(T)$ peak at the spin–flop transition decrease with increasing frequency of the oscillating magnetic field component. Away from the AF–SF phase transition $\chi'(T)$ appears to be frequency independent. The frequencies 29.2 and 2085 Hz were deliberately chosen in order to observe the isothermal χ_T and adiabatic χ_s limits of χ' for the low-frequency relaxation discussed in section 4.2. The observed frequency dependence of $\chi'(T)$ clearly shows that the low-frequency relaxation does not occur in the ordered AF and SF phases, thus corresponding to the result in section 4.1.1. The temperature half width ΔT at half height of the $\chi'(T)$ peaks increases from its minimum of $\sim$0.012 K for $\chi_T(T)$ to its maximum value of $\sim$0.023 K for $\chi_s(T)$.

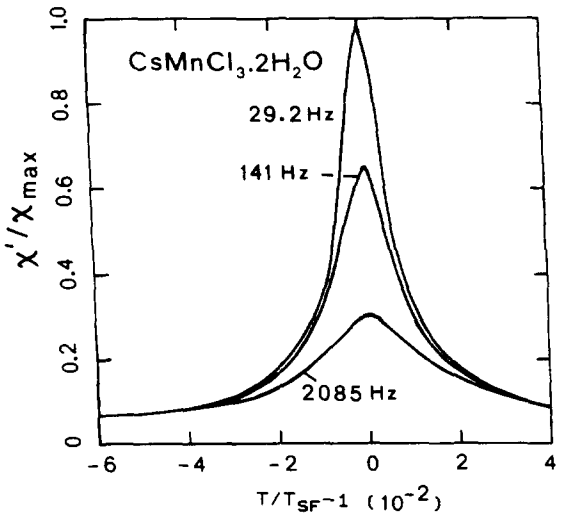

Fig. 2. Temperature dependence of the dispersion χ' near the spin–flop transition $H_{SF} = 1.44 \times 10^6$ A m^{-1}, $T_{SF} = 2.00$ K for $CsMnCl_3 \cdot 2H_2O$. χ_{max} is the maximum isothermal susceptibility at the phase transition.

4.2. Relaxation at the spin–flop transition

4.2.1. Shape of the Argand diagrams

With the $CsMnCl_3 \cdot 2H_2O$ single crystal in liquid helium at temperatures below T_λ, the frequency dependence of the dynamic susceptibility $\chi(\omega)$ at the spin–flop transition was characterized by fairly perfect semi-circular Argand ($\chi''(\omega)$–$\chi'(\omega)$) diagrams. This behaviour is in accordance with the ideal behaviour (Casimir–du Pré theory) of $\chi'(\omega)$ and $\chi''(\omega)$ given by the equations

$$\chi'(\omega) = \chi_T - \omega\tau B(\omega), \tag{3}$$

$$\chi''(\omega) = B(\omega), \tag{4}$$

where

$$B(\omega) = \omega\tau(\chi_T - \chi_s)/(1 + \omega^2\tau^2). \tag{5}$$

Consequently the time constants τ_{dis} and τ_{abs} derived from the frequencies of the $\chi'(\omega)$ inflection point and the $\chi''(\omega)$ maximum, respectively, are equal to the intrinsic relaxation time τ. From the measurements above T_λ, however, flattened dispersion $\chi'(\omega)$ and broadened absorption $\chi''(\omega)$ curves, resulting in non-semicircular Argand diagrams, were obtained. In this case τ_{dis} and τ_{abs} are not equal to τ. Typical Argand diagrams from measurements above and below T_λ are given in fig. 3. The semi-circular Argand diagram A was obtained at the spin–flop transition

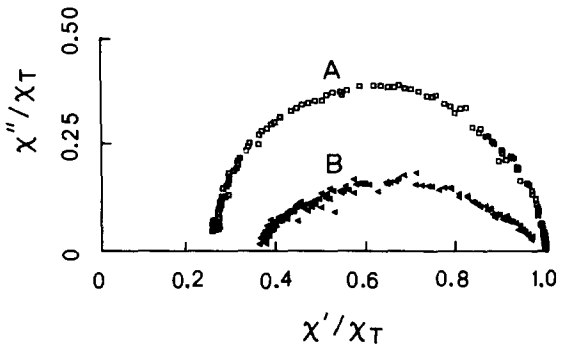

Fig. 3. Typical Argand (χ''–χ') diagrams for the relaxation at the spin–flop transition obtained from measurements on a $CsMnCl_3 \cdot 2H_2O$ single crystal in contact with liquid helium (A) at $T = 1.894$ K, $H = 1.4288 \times 10^6$ A m^{-1} and (B) at $T = 2.358$ K, $H = 1.4624 \times 10^6$ A m^{-1}, below and above T_λ, respectively.

$H = 1.4288 \times 10^6$ A m^{-1}, $T = 1.894$ K and the non-semicircular Argand diagram B is the result of a measurement above T_λ for $T = 2.358$ K and $H = 1.4624 \times 10^6$ A m^{-1}. Although both measurements were performed over the same frequency range (0.1 Hz to 3 kHz) curve B shows that the isothermal limit χ_T was not reached. A quantitative measure of how much an Argand diagram has deviated from the ideal semi-circular shape is given by a deviation parameter d defined by

$$d = 1 - 2\chi''_{max}/(\chi_T - \chi_s). \quad (6)$$

For the semi-circular shape, $d = 0$. In the case of the Argand diagram B, in fig. 3, $d \sim 0.52$.

4.2.2. Field dependence of the relaxation rate τ^{-1}

At constant temperature the low-frequency relaxation rate in the AF–SF transition region depends on the magnetic field H. From the frequency dependence (fig. 4) of $\chi'(\omega)$ and $\chi''(\omega)$ measured at $T = 1.955$ K for $H = 1.4338 \times 10^6$ A m^{-1}, 1.4334×10^6 A m^{-1} and 1.4331×10^6 A m^{-1}, with the corresponding $\tau^{-1} = 7.85 \times 10^2$ s^{-1}, 1.00×10^3 s^{-1} and 1.35×10^3 s^{-1}, respectively, it is observed that τ^{-1} varies rapidly with H. In addition both the adiabatic χ_s and the isothermal χ_T susceptibilities, as well as their ratio χ_s/χ_T, change with the field. In particular χ_s/χ_T and τ^{-1} exhibit similar field dependences

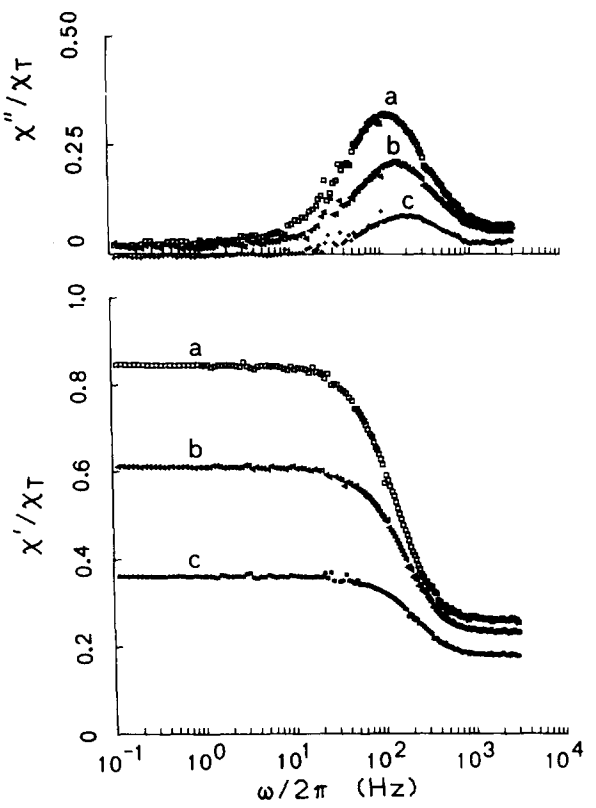

Fig. 4. Effect of small magnetic field changes on the frequency dependence of χ' and χ'' in the AF–SF intermediate state of $CsMnCl_3 \cdot 2H_2O$ at $T = 1.955$ K. (a) $H = 1.4338 \times 10^6$ A m^{-1}, $\tau^{-1} = 7.85 \times 10^2$ s^{-1}. (b) $H = 1.4334 \times 10^6$ A m^{-1}, $\tau^{-1} = 10.0 \times 10^2$ s^{-1}. (c) $H = 1.4331 \times 10^6$ A m^{-1}, $\tau^{-1} = 13.5 \times 10^2$ s^{-1}.

such that for a given value of χ_s/χ_T at constant temperature, the relaxation rate τ^{-1} is the same irrespective of the applied magnetic field within the transition region. For example in fig. 5, where τ^{-1} and χ_s/χ_T are plotted against H at $T = 1.955$ K, the relaxation rate is 0.95×10^3 s^{-1} for $\chi_s/\chi_T = 0.35$ at both $H = 1.4334 \times 10^6$ A m^{-1} and $H = 1.4342 \times 10^6$ A m^{-1}. Using the thermodynamic identity $\chi_s/\chi_T = C_M/C_H$ and the relation $\tau^{-1} = \alpha/C_H$, where α is a proportionality factor and C_M and C_H are the magnetic specific heat capacities at constant magnetization and constant field respectively, we obtain the equation

$$\tau^{-1} = (\alpha/C_M)\chi_s/\chi_T. \quad (7)$$

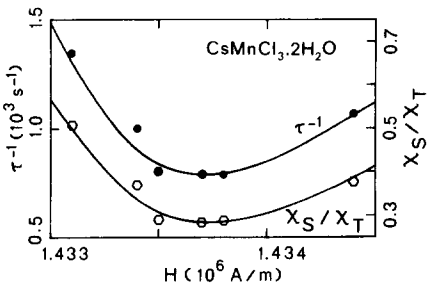

Fig. 5. Magnetic field dependence of τ^{-1} and χ_s/χ_T in a small field interval $\sim 0.5\,\Delta H$ around $H = H_{SF}$ at $T = 1.955$ K.

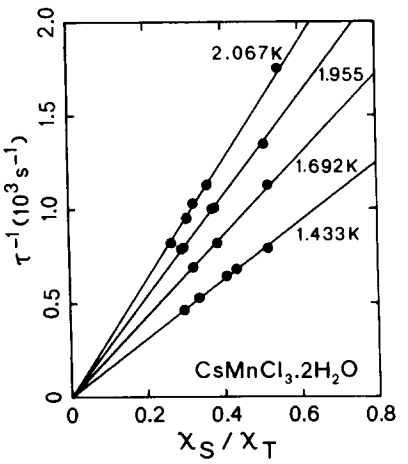

Fig. 6. Variation of τ^{-1} with χ_s/χ_T at the spin–flop transition of $CsMnCl_3 \cdot 2H_2O$.

Then a plot of τ^{-1} against χ_s/χ_T at constant T should yield a straight line with slope α/C_M and intercept at origin of co-ordinates, provided α/C_M is independent of H. A linear dependence of τ^{-1} on χ_s/χ_T is indeed found as shown in fig. 6 at several temperatures. These results show that α/C_M is independent of H at constant temperature.

4.2.3. Temperature dependence of the relaxation rate τ^{-1}

In our previous study of relaxation at the spin–flop transition of $CsMnBr_3 \cdot 2H_2O$ [9], the temperature dependence of τ^{-1} was determined from the frequency dependence of $\chi(\omega)$ at the susceptibility $\chi(H)$ peak at which the quantity $\chi_s/\chi_T \sim 0.4$ was found to be nearly independent of temperature. From the present relaxation experiments on $CsMnCl_3 \cdot 2H_2O$ it has been found that also for this compound χ_s/χ_T is temperature independent, although the actual measurements at the $\chi(H)$ peak may be hampered by its sharpness. When this behaviour of χ_s/χ_T is considered together with eq. (7) in section 4.2.2., it becomes obvious that the temperature dependence of τ^{-1} is simply that due to the variation of the field-independent factor α/C_M, that is the slope of the τ^{-1} versus χ_s/χ_T in fig. 6. This shows that it is not necessary to measure $\chi(\omega)$ at the $\chi(H)$ peak in order to determine the temperature dependence of τ^{-1}. Therefore τ^{-1} was evaluated at each temperature for a fixed value of χ_s/χ_T. An example of the results obtained is displayed in fig. 7 by the log-linear plot of τ^{-1} against T^{-1} for $\chi_s/\chi_T = 0.42$. At temperatures below T_λ the $\tau^{-1}(T)$ data yielded an exponential dependence. Above T_λ the substantial environmental influence on $\chi'(\omega)$ and $\chi''(\omega)$ was observed to give values of τ_{abs}^{-1} much lower than the intrinsic relaxation rate τ^{-1} (see section 4.3). Strictly speaking, fig. 7 shows the observed temperature dependence of τ_{abs}^{-1}.

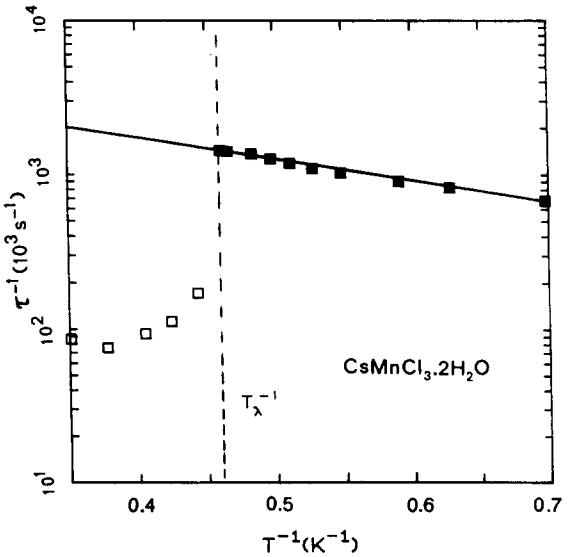

Fig. 7. A typical example of the dependence of the relaxation rate τ^{-1} on the reciprocal temperature T^{-1} for $\chi_s/\chi_T = 0.42$ at the spin–flop transition. The straight line represents $\tau^{-1} \propto \exp(-E/kT)$ with $E/k = 3.19$ K.

However, as indicated earlier (section 4.2.1), the data for $T < T_\lambda$ correspond to $\tau^{-1}(T)$, whereas the data at $T > T_\lambda$ does not.

The activation energy E for the relaxation process and the coefficient ω_0 were obtained by fitting the $\tau^{-1}(T)$ data at $T < T_\lambda$ to eq. (1). Fig. 8 shows the variation of E/k and ω_0 with χ_s/χ_T. It is observed that E/k is independent of χ_s/χ_T and has a value, 3.19 ± 0.04 K, approximately equal to $|J_a/k|$ for $CsMnCl_3 \cdot 2H_2O$. This result gives the same relationship between E/k and J_a/k as that found for $CsMnBr_3 \cdot 2H_2O$ in ref. [9]. The parameter ω_0 increases linearly with χ_s/χ_T according to the empirical formula.

$$\omega_0 = d(\chi_s/\chi_T), \tag{8}$$

where $d = 1.41 \times 10^4\ s^{-1}$. By combining eqs. (1), (7) and (8) it can be shown that

$$\alpha/C_M = d \exp(-E/kT). \tag{9}$$

4.2.4. Variation of τ^{-1} with χ_s/χ_T from $\chi'(\omega)$ versus T curves

As a further check on the variation of τ^{-1} with χ_s/χ_T, the $\chi'(\omega)$ measured as a function of temperature at constant magnetic field (section 4.1.2.) was analysed by using eq. (3). Three simultaneous equations in $\chi'(\omega_n)$ and ω_n, for $n = 1, 2$ and 3, were set up in order to calculate τ, χ_s and χ_T. This analysis, however, has limited scope because a non-trivial or physically meaningful solution of such a set of equations is only found for $\chi'(\omega_i) \neq \chi'(\omega_j)$ when $\omega_i \neq \omega_j$. Where this condition is valid, the anticipated linear dependence of τ^{-1} on χ_s/χ_T was found.

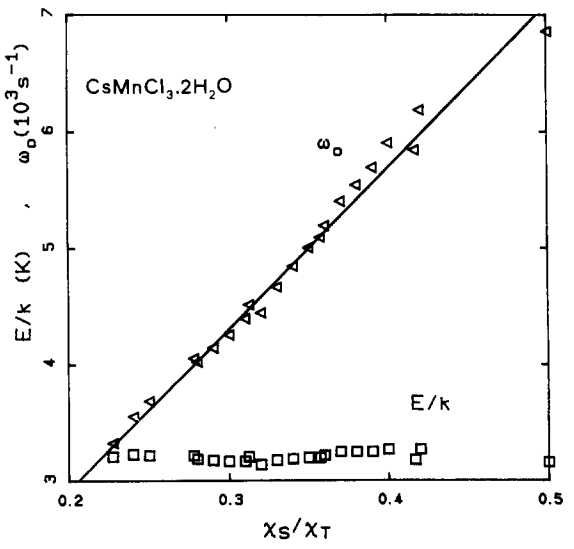

Fig. 8. The activation energy E/k and the coefficient ω_0 as functions of the susceptibility ratio χ_s/χ_T at the spin–flop transition of $CsMnCl_3 \cdot 2H_2O$.

4.3. Application of the thermal conduction model (TCM)

In section 4.2.1. it was shown that the observed behaviour of $\chi(\omega)$ for a sample in contact with liquid helium at temperatures above T_λ cannot be described by the Casimir–du Pré equations. As a result the intrinsic relaxation time τ cannot be readily obtained from such curves. In this section we use the thermal conduction model [13] (TCM) to describe the frequency dependence of $\chi(\omega)$ and therefore relate these curves to the expected intrinsic relaxation time τ at $T > T_\lambda$. Thus according to TCM the effects of thermal properties of the environment and sample on the $\chi(\omega)$ curves is accounted for when $\chi'(\omega)$ and $\chi''(\omega)$ are given by

$$\chi'(\omega) = \chi_T - \omega\tau B(\omega) \cdot (1 + W_1 - W_2/\omega\tau) \tag{10}$$

and

$$\chi''(\omega) = B(\omega) \cdot (1 + W_1 + W_2\omega\tau), \tag{11}$$

with $B(\omega)$ given by eq. (5). Here W_1 and W_2 are the real and imaginary parts of the geometry-dependent complex function W,

$$W = W(D, F, P, Q, R, S, \omega, \tau) = (P/L^2)(L - Z^{-1})/(1 + i\omega\tau), \tag{12}$$

where

$$L = B(\omega) \cdot [1 + i(1 + \omega^2\tau^2 + D)/\omega\tau D]P \tag{13}$$

and Z is a function describing the heat transport

properties in the sample and the environment. The dimensionless group-variables D, F, P, Q, R and S are defined in table III. The shape of the $CsMnCl_3 \cdot 2H_2O$ crystal used is approximately plate-like with thickness $2r = 0.7$ mm, in which case the function Z is written as

$$Z = Q + (1 - i)S/(2PRS\omega\tau)^{1/2} + \coth(L^{1/2})/L^{1/2} \tag{14}$$

When $W_1 = W_2 = 0$, eqs. (10) and (11) reduce to the Casimir–du Pré relations. When the sample is thermally isolated, $Z^{-1} = 0$.

In order to calculate values for the dimensionless group parameters we used the heat capacity C_B and thermal conductivity λ_B for liquid helium [36] and the lattice thermal conductivity of $CsMnCl_3 \cdot 2H_2O$ at the spin–flop transition [37]. The thermal resistance R_K at the crystal–bath interface was taken as zero while the simple Debye T^3-law was used to estimate the lattice heat capacity C_L. With this information, together with the susceptibility measurements, only F, Q and S can be calculated. The remaining parameters D, P and R require the knowledge of the constant field magnetic heat capacity C_H. Since there is no C_H data for $CsMnCl_3 \cdot 2H_2O$ at the spin–flop transition, C_H was taken as a variable parameter while assuming that the exponential temperature dependence of τ found below T_λ can be extended to temperatures above T_λ. It is now possible to evaluate D, P and R as well, and therefore the $\chi'(\omega)$ and $\chi''(\omega)$ curves. In the comparison between the calculated and experimental $\chi(\omega)$ curves the best agreement was found for C_H values ranging from 11 J mol^{-1} K^{-1} at $T = 2.23$ K to 15 J mol^{-1} K^{-1} at $T = 2.65$ K, which are comparable to the only available experimental molar heat capacity C_H at the AF–SF transition [38] for the compound $MnCl_2 \cdot 4H_2O$. Fig. 9 shows an example of the agreement found between the experimental data and theoretical (TCM) calculations (curves a) at $T = 2.36$ K. The anticipated intrinsic relaxation process is represented by curves b calculated with eqs. (3) and (4) for $\tau = 0.616 \times 10^{-3}$ s, which is about 17 times smaller than the $\tau_{abs} \sim 10.5 \times 10^{-3}$ s.

Table III
The dimensionless group parameters of the thermal conduction model

$D = C_H/C_L$
$F = 1 - \chi_s/\chi_T = 1 - C_M/C_H$
$P = r^2\alpha/\lambda_L$, where $\alpha = C_H/\tau$
$Q = \lambda_L R_K/r$
$R = C_B/C_H$
$S = \lambda_L/\lambda_B$

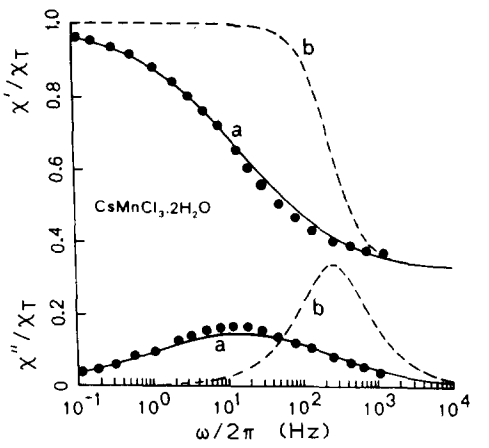

Fig. 9. Comparison between the experimental data and theoretical (TCM) calculations (curves a) of $\chi'(\omega)$ and $\chi''(\omega)$ for $CsMnCl_3 \cdot 2H_2O$ at $H = 1.4624 \times 10^6$ A m^{-1}, $T = 2.358$ K. The expected intrinsic relaxation behaviour is represented by the curves b for $\tau = 0.616 \times 10^{-3}$ s.

5. Discussion

In this section we discuss the general behaviour of the dynamic susceptibility, the domain structure, the thermodynamics and the relaxation phenomena at the spin–flop transition. A comparison between metamagnetic and spin–flop systems is given at appropriate places.

5.1. Dynamic susceptibility behaviour at the phase transition

From the field and temperature dependence of the dynamic susceptibility at several frequencies it has been shown that the low-frequency relax-

ation, found at the spin–flop transition of $CsMnCl_3 \cdot 2H_2O$, does not exist in the low-field AF and high-field SF phases. A similar behaviour of the dynamic susceptibility has also been observed in $CsMnBr_3 \cdot 2H_2O$ [9]. Relaxation within the ordered domains (paraprocess), where $\tau^{-1} > 10^5\,s^{-1}$ [39], is at least 10^2–10^3 times faster than the domain-wall relaxation at first-order phase transitions. At 2.0 K the relaxation rates at the spin–flop transition of $CsMnBr_3 \cdot 2H_2O$ and $CsMnCl_3 \cdot 2H_2O$ and at the metamagnetic transition of $[(CH_3)_3NH]\,CoCl_3 \cdot 2H_2O$ [40] are $\sim 4 \times 10^3\,s^{-1}$, $\sim 1 \times 10^3\,s^{-1}$ and $\sim 0.4 \times 10^3\,s^{-1}$, respectively. In the case of the compounds $CoBr_2 \cdot 2H_2O$ and $CoCl_2 \cdot 2H_2O$ which exhibit two metamagnetic transitions at H_{c_1} and H_{c_2}, the relaxations rates are $\leq 10^{-1}\,s^{-1}$ and $\leq 3 \times 10^3\,s^{-1}$ at the first (H_{c_1}) and the second (H_{c_2}) transitions respectively [41, 42].

The adiabatic limit of the susceptibility in the region of the spin–flop transition is expected to be $\chi_s = (1-\epsilon)\chi_{AF} + \epsilon\chi_{SF}$ where $0 \leq \epsilon \leq 1$ and χ_{AF} and χ_{SF} are the susceptibilities in the AF and SF phases. This would be the case if the low-frequency domain-wall relaxation and the high-frequency paraprocess were the only relaxation processes at the transition. However experimentally χ_s for the low-frequency relaxation is considerably larger than χ_{AF} or χ_{SF}. Our measurements indicate that there is an additional relaxation process at higher frequencies, but with a lower relaxation rate than that for the paraprocess. This second relaxation process should also be related to domain-wall motion. However further investigations are required in order to understand this process.

At a first-order magnetic phase transition one expects the maximum isothermal susceptibility (here denoted by χ_{max}) to be equal to the reciprocal of the demagnetization factor D. For a uniformly magnetized ellipsoidal (constant D) crystal sample placed in a uniform magnetic field, this would be the case. However it is observed that χ_T has a maximum value less than D^{-1} and varies continuously over a field interval larger than $D \cdot \Delta M$, where $\Delta M = (\chi_{SF} - \chi_{AF})H_{SF}$ is the magnetization change over the transition. For $CsMnCl_3 \cdot 2H_2O$ the observed χ_{max} is about $60\chi_{AF}$. At 3 K, $\chi_{AF} = \chi_0 \approx 2 \times 10^{-3}$ (S.I.) [20] so that $\chi_{max} \approx 0.1$, about 50 times less than $D^{-1} \approx 5$ for the crystal. At this temperature $\chi_{SF} = \chi_\perp = 4.7 \times 10^{-3}$ [20] and $H_{SF} = 1.5 \times 10^6\,A\,m^{-1}$ so that $D \cdot \Delta M \approx 8 \times 10^2\,A\,m^{-1}$ whereas the full extent of the spin–flop transition (see fig. 1) is well over $4 \times 10^4\,A\,m^{-1}$ about 50 times larger than $D \cdot \Delta M$. De Jongh et al. [43] suggest that in low-dimensional systems the extent of the transition beyond $D \cdot \Delta M$ may be explained by considering the non-linear contributions to M arising from the thermally excited π-solitons. In this theory the π-soliton near the spin-flop transition can be considered as an excitation of a small portion of one phase (AF or SF) into the other. At $H = H_{SF}$ the soliton contribution to M is zero but it is positive at $H < H_{SF}$ and negative at $H > H_{SF}$, so that the total M is expected to exhibit a gradual transition over an extended field interval. We have not pursued this subject further because our measurements were performed on a crystal with non-ellipsoidal shape.

5.2. Domain-wall structure at the spin–flop transition

In the absence of an external magnetic field or weak ferromagnetism, an antiferromagnet should not form domains. Nevertheless a domain structure in an antiferromagnet may exist due to the kinetics of crystal growth or of a phase transition. The reason for domain-wall formation at the spin–flop transition has already been considered in the introductory part of this paper. The wall at the spin–flop transition lies with its surface parallel to the easy axis. In a sample with purely uniaxial anisotropy there are numerous equivalent planes parallel to the preferred axis. For an orthorhombic system, however, the anisotropy in the plane perpendicular to the easy axis limits the degree of freedom of orientation of the wall in comparison to the uniaxial case. The domain-wall width depends strongly on the strength of the anisotropy but is not expected to be appreciably influenced by the kind of anisotropy. Therefore we apply the calculations of Hubert and Bar'yakhtar et al. [1] for a uniaxial crystal to the orthorhombic $CsMnCl_3 \cdot 2H_2O$ system to obtain the wall width $\delta = 2\sqrt{2a/\chi_\perp}$ as

$\sim 10^3 a$ where a is the separation between two neighbouring magnetic ions and $\chi_\perp \sim 10^{-3}$. This is a very thick wall in comparison to the domain wall at a metamagnetic transition, which is constrained by the strong Ising anisotropy to a few lattice spacings only.

5.3. Thermodynamics

Using the thermodynamic relations $\chi_s/\chi_T = C_M/C_H$ and $\tau^{-1} = \alpha/C_H$ we have been able to explain well the dependence of τ^{-1} on the magnetic field at the spin–flop transition. We have also found C_M/α to be a field-independent function that decreases exponentially with increasing temperature. These results are probably applicable to other spin–flop systems similar to $CsMnCl_3 \cdot 2H_2O$.

Since C_H is directly coupled to χ_T and τ, its behaviour at phase transitions should correspond to the variations in χ_T and τ. In particular we expect C_H to exhibit a peak at the phase transition similar to those observed in τ and χ_T. For example at the AF–PM boundary C_H and both τ and χ_T exhibit peaks (see refs. [15] and [38] for example). At the spin–flop transition of $CsMnCl_3 \cdot 2H_2O$ we have observed peaks in τ and χ_T and thus we expect a similar behaviour in C_H. There are no heat capacity data for this compound at the AF–SF phase transition. The only available C_H data are those for $MnCl_2 \cdot 4H_2O$ in ref. [38] which however do not indicate any abrupt change as the AF–SF boundary is crossed at constant applied field. In view of this contradiction we suggest further specific heat studies at spin–flop transitions.

5.4. Relaxation

For both $CsMnCl_3 \cdot 2H_2O$ and $CsMnBr_3 \cdot 2H_2O$, the low-frequency domain-wall relaxation rate at the spin–flop transition has been found to be an exponential function of temperature ($T < T_\lambda$), with the activation energy nearly equal to the magnitude of the intrachain exchange interaction constant. In the case of $CsMnCl_3 \cdot 2H_2O$, the apparent deviation from exponential behaviour at $T > T_\lambda$ has been explained in terms of the influence of thermal properties of liquid helium and the crystal on the frequency dependence of susceptibility. In this analysis C_H was taken as a variable parameter in order to fit the theoretical curves to the experimental data as there are no heat capacity data of $CsMnCl_3 \cdot 2H_2O$ at the spin–flop transition.

In the Tinkham model of a metamagnetic transition the activation energy for domain-wall motion is equal to $4zJS^2$, the energy required to reverse the orientation of a single spin against its z nearest neighbours in the chain. In the case of a spin $S = 1/2$ metamagnet, the activation energy is simply equal to zJ and this is found experimentally ($z = 1$, see table IV). However there are no experimental results on compounds with values of S larger than 1/2.

If we apply the same principle to a spin–flop system, such as $CsMnCl_3 \cdot 2H_2O$, we would obtain an activation energy of $12.5zJ_a$, which is far too large in comparison to the experimental results. The Tinkham model may be realistic in the case of metamagnets with small domain-wall widths but not for the spin–flop systems where the corresponding wall widths are comparatively large. For the latter case an analogous descrip-

Table IV
Comparison between the wall motion activation energy E and the intrachain exchange constant J in spin–flop and metamagnetic systems

System type	Crystal sample	J/k (K)	E/k (K)	Source
Spin flop	$CsMnCl_3 \cdot 2H_2O$	−3.20	3.19 ± 0.04	this paper
Spin flop	$CsMnBr_3 \cdot 2H_2O$	~ -3.0	~3.6	[9]
Metamagnet	$[(CH_3)_3NH]CoCl_3 \cdot 2H_2O$	13	8.5, 17.5	[40]

tion would be that wall motion is initiated by rotation of a spin over an angle much less than 90°. Then the neighbouring spins in the chain are successively induced to rotate through equally small angles. In this process the energy involved is less than that for one complete 90° rotation. This gives a partial qualitative explanation of the results found. However further experimental work on spin–flop and metamagnetic systems with different values of J and S, as well as a theoretical study of the origin of this behaviour are necessary in order to answer the remaining questions.

References

[1] A. Hubert, Theorie der Domänenwände in geordneten Medien (Springer–Verlag, Berlin, 1974);
V.G. Bar'yakhtar, A.E. Borovik and V.A. Popov, JETP Lett. 9 (1969) 391.

[2] A.R. King and D. Paquette, Phys. Rev. Lett. 30 (1973) 662.

[3] V.G. Baryakhtar, A.A. Galkin, E.P. Stefanovskii and V.T. Telepa, Sov. Phys. Solid State 18 (1976) 1775.

[4] V.V. Eremenko, K.L. Dudko and N.V. Gapon, J. Appl. Phys. 50 (1979) 7754;
V.P. Novikov, V.V. Eremenko and I.S. Kachur, Sov. Phys. JETP 55 (1982) 327.

[5] P.B. Johnson, J.A. Rayne and S.A. Friedberg, J. Appl. Phys. 50 (1979) 1853; see also references 2–4, 30–32, 37 and 38.

[6] J.A. Overweg, H.J.M. ter Brake, J. Flokstra and G.J. Gerritsma, J. Phys. E: Sci. Instrum. 16 (1983) 1247.

[7] G.J. Gerritsma, W.J. van Weezep, J.A. Overweg and J. Flokstra, J. Phys. E: Sci. Instrum. 16 (1983) 270.

[8] H. Rohrer, AIP Conf. Proc. No. 24 (1974) 268.

[9] M. Chirwa, J. Top and J. Flokstra, Physica 123B (1983) 53.

[10] M. Tinkham, Phys. Rev. 188 (1969) 967.

[11] For reviews on low-dimensional magnetic systems see:
L.J. de Jongh and A.R. Miedema, Adv. Phys. 23 (1974) 1;
M. Steiner, J. Villain and C.G. Windsor, Adv. Phys. 25 (1976) 87.

[12] H.B.G. Casimir and F.K. du Pré, Physica 5 (1938) 507.

[13] J. Flokstra, G.J. Gerritsma, G.A. Hartemink and L.C. van der Marel, Physica 77 (1974) 99.

[14] J. Flokstra, G.J. Gerritsma and L.C. van der Marel, Physica 94B (1978) 53;
G.J. Gerritsma, J. Flokstra, G.A. Hartemink, J.J.M. Scholten, A.J.W.A. Vermeulen and L.C. van der Marel, Physica 95B (1978) 173.

[15] H.A. Groenendijk, J. Flokstra and A.J. van Duyneveldt, Physica 112B (1982) 33.

[16] S.J. Jensen, P. Andersen and S.E. Rasmussen, Acta Chem. Scand. 16 (1962) 1890.

[17] R.D. Spence, W.J.M. de Jonge and K.V.S. Rama Rao, J. Chem. Phys. 51 (1969) 4694.

[18] J. Skalyo Jr., G. Shirane, S.A. Friedberg and H. Kobayashi, Phys. Rev. B2 (1970) 1310.

[19] T. Smith and S.A. Friedberg, Phys. Rev. 176 (1968) 660.

[20] H. Kobayashi, I. Tsujikawa and S.A. Friedberg, J. Low Temp. Phys. 10 (1973) 621.

[21] A.C. Botterman, W.J.M. de Jonge and P. de Leeuw, Phys. Lett. 30A (1969) 150;
A.C. Botterman, Ph.D. Thesis, Eindhoven University of Technology (1976).

[22] K. Kopinga, T. de Neef and W.J.M. de Jonge, Phys. Rev. B11 (1975) 2364.

[23] K. Kopinga, Phys. Rev. B16 (1977) 427.

[24] J. Skalyo Jr., G. Shirane, S.A. Friedberg and H. Kobayashi, Phys. Rev. B2 (1970) 4632.

[25] M.J. Hennessy, C.D. McElwee and P.M. Richards, Phys. Rev. B7 (1973) 930.

[26] F. Ferrieu, Phys. Lett. 49A (1974) 253.

[27] T. Iwashita and N. Uryu, J. Phys. Soc. Jap. 39 (1975) 1226.

[28] W.J.M. de Jonge, K. Kopinga and C.H.W. Swüste, Phys. Rev. B14 (1976) 2137.

[29] I.R. Jahn, J.B. Merkel, H. Ott and J. Herrmann, Solid State Comm. 19 (1976) 151.

[30] E. Vélu, J.P. Renard and G. Corbel, J. de Physique 39 (1978) C6-717.

[31] G.J. Butterworth, J.A. Woollam and P. Aron, Physica 70 (1973) 547;
P.R. Aron, J.A. Woollam and G.J. Butterworth, Phys. Lett. 35A (1971) 422;
G.J. Butterworth and J.A. Woollam, Phys. Lett. 29A (1969) 259.

[32] W.J.M. de Jonge, J.P.A.M. Hijmans, F. Boersma, J.C. Schouten and K. Kopinga, Phys. Rev. B17 (1978) 2922;
F. Boersma, Ph.D. Thesis, Eindhoven University of Technology (1981).

[33] E. Vélu and R. Mégy, J. Magn. Magn. Mater. 15–18 (1980) 1017;
E. Vélu, R. Mégy and J. Seiden, Phys. Rev. B27 (1983) 4429;
E.Vélu, R. Mégy, J. Seiden and J.P. Renard, J. Magn. Magn. Mater. 31–34 (1983) 1069.

[34] K. Nagata, Y. Tazuke and K. Tsushima, J. Phys. Soc. Jap. 32 (1972) 1486.

[35] K. Nagata and Y. Tazuke, Phys. Lett. 31A (1970) 293.

[36] J. Wilks, The Properties of Liquid and Solid Helium (Clarendon Press, Oxford, 1967).

[37] J.A.H.M. Buys, J.P.M. Smeets and W.J.M. de Jonge, J. Magn. Magn. Mater. 15–18 (1980) 923.

[38] W.F. Giauque, R.A. Fisher, E.W. Hornung and G.E. Brodale, J. Chem. Phys. 53 (1970) 1474.

[39] D.L. Huber, Phys. Rev. B3 (1971) 836.
[40] H.A. Groenendijk and A.J. van Duyneveldt, Physica 115B (1982) 41.
[41] A. van der Bilt and A.J. van Duyneveldt, Physica 95B (1978) 305.
[42] Y. Kuramitsu, K. Amaya and T. Haseda, J. Phys. Soc. Jap. 33 (1972) 83;
A.J. van Duyneveldt and J. Soeteman, Phys. Stat. Sol. (a) 16 (1973) K17.
[43] L.J. de Jongh, J. Appl. Phys. 53 (1982) 8018;
D. Bloch, J. Voiron and L.J. de Jongh, High Field Magnetism, M. Date, ed. (North-Holland, Amsterdam, 1983) p. 19.